Modeling of Muscle Wrapping Phenomenon: A Geometric Method Based on Tangency Constraints

Iram Muñoz-Pepi, Nadia Garcia-Hernandez, and Vicente Parra-Vega, *Member, IEEE*

***Abstract*—Musculoskeletal simulations have become an essential tool for surgical planning and clinical evaluation of movement. Accurate simulations of muscle-tendon paths in musculoskeletal models promote better predictions of muscle forces and, therefore, joint torques. A precise description of a muscle-tendon unit behavior should consider the wrapping phenomenon around bones. State-of-the-art muscle wrapping methods do not guarantee continuity along the path, which may result in unrealistic solutions. Moreover, many use the well-known Newton-Raphson method, discarding other methods to solve the problem. This article presents a muscle wrapping formulation based on tangency constraints that, unlike other methods, guarantees $\mathcal{C}^1$ continuity along the path over n parametric surfaces. We first test our formulation over one cylinder to compare the numerical efficiency considering the Newton-Raphson and two Quasi-Newton (Broyden–Fletcher–Goldfarb–Shanno and Broyden) methods under two cases: 1) wrapping state all the time, and 2) from/to a wrapping to/from a non-wrapping state. Results show that all yields well-posed solutions according to the tangency constraints, and that Broyden's method is the fastest to converge. Finally, a simulation of muscle wrapping over two cylinders was performed using Broyden's method considering the transition from/to a wrapping to/from a non-wrapping state, resulting also in $\mathcal{C}^1$ muscle paths.**

***Index Terms*—Tendon/Wire Mechanism, Modeling and Simulating Humans, Muscle Wrapping, Muscle-tendon Path, Geodesics.**

I. Introduction

NOWADAYS, applications of simulations of the human musculoskeletal system range from rehabilitation studies to planning interventions [1] and are of great interest in biomechanics to evaluate movement driven by muscle dynamics [2]. The construction of accurate human musculoskeletal models is essential for a better estimation of the force generated by muscle-tendon units. Muscle force is often estimated from the force-length-velocity properties of muscle fibers and the elastic properties of tendons using Hill-type actuation models [3]; in both upper [4] and lower [5] limb musculoskeletal models. To better estimate the muscle-tendon force from the Hill-type model, which also affects the assessment of joint moments, the modeling of muscle-tendon behavior must consider the muscle-wrapping phenomenon. This phenomenon occurs when a muscle interferes with skeletal structures, such as bones, causing the muscle-tendon to wrap around a rigid body. An example of muscle wrapping is shown in Fig. 1, where the lateral triceps head wraps around the elbow joint for a specific range of motion. During the wrapping state, the muscle's line of action is no longer a simple straight line but a curved path over the wrapped surface. Therefore, it is required to calculate the muscle-tendon path during muscle-wrapping, which becomes a challenging process. Henceforth, developing feasible algorithms that compute muscle-tendon force involving the physiological muscle wrapping phenomenon requires precise models and calculations of the continuous muscle-tendon path, its length, velocity, and moment arms.

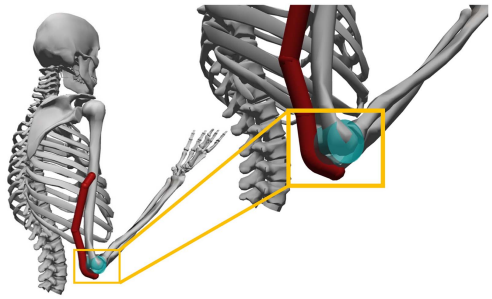

Fig. 1. Snapshot (taken from OpenSim [2]) showing the lateral muscle-tendon unit of the triceps head wrapping path over a cylindrical constraint surface (cyan color) representing the anatomical elbow joint.

Several works have implemented geodesic-based methods to compute the shortest muscle-tendon path. Some have used a discrete approach to improve the efficiency of simulations [6], [7], but often at lower muscle velocity accuracy, in contrast to the solution based on the continuous computation over different surfaces [8]. Moreover, the solution is discontinuous for some configurations at the connection points (between the curved and straight line segments), causing a jerky motion in the muscle path. This problem arises from the constraints formulation subject to the geodesic's normal and binormal vectors. All this

Manuscript received 6 March 2023; accepted 14 August 2023. Date of publication 7 September 2023; date of current version 19 September 2023. This letter was recommended for publication by Associate Editor A. Seth and Editor A. Bera upon evaluation of the reviewers' comments. The work of Iram Muñoz-Pepi was supported by the National Council of Humanities, Science and Technology of Mexico (CONAHCYT) through the Scholarship under Grant CVU#861816. *(Corresponding author: Nadia Garcia-Hernandez.)*

Iram Muñoz-Pepi and Vicente Parra-Vega are with the Department of Robotics and Advanced Manufacturing, Research Center for Advanced Studies, Ramos Arizpe, Coahuila 25900, Mexico (e-mail: iram.munoz@cinvestav.mx; vparra@cinvestav.mx).

Nadia Garcia-Hernandez is with the Department of Robotics and Advanced Manufacturing, Research Center for Advanced Studies, Ramos Arizpe, Coahuila 25900, Mexico, and with the Rehab Technologies Lab, Italian Institute of Technology, 16163 Genova, Italy, and also with the National Council of Humanities, Science and Technology of Mexico, Mexico City 03940, Mexico (e-mail: nadia.garcia@iit.it, nadia.garcia@cinvestav.mx).

This letter has supplementary downloadable material available at https://doi.org/10.1109/LRA.2023.3313027, provided by the authors.

Digital Object Identifier 10.1109/LRA.2023.3313027

highlight the need for new methods that work for different wrapping surfaces to solve the problem of muscle-tendon wrapping path discontinuity and the computation of muscle-tendon velocity. These will provide consistent and realistic muscle force.

This letter presents an efficient muscle wrapping method that promotes a realistic computation of muscle path over n parametric surfaces and the muscle velocity for accurate muscle force estimation. The proposed method utilizes the local tangent components of each geodesic to formulate tangency constraints, thus ensuring continuity along the muscle-tendon path to avoid non-realistic wrapping. Simulations were performed to first test the proposed wrapping method over one cylinder and to compare the efficiency of three different numerical methods. In this simulation there were two scenarios: 1) wrapping over a cylindrical surface and 2) transitioning from/to wrapping a cylindrical surface to/from non-wrapping (taking into account the cylinder non-wrapping condition presented in [9]). A simulation of a muscle-tendon wrapping over two cylinders was also performed to show the scalability of the proposed wrapping method. For this last simulation, the most efficient numerical method found in the first test was used.

II. Background

Most works on muscle-wrapping modeling have been addressed through finite element formulations assuming massless wire models, showing high fidelity at a high computational cost [10], thus making integration with other non-finite elements of biomechanical or dynamic models difficult. The massless wire assumption neglects the muscle's inertial parameters to facilitate addressing straight and curved-line segments. These models are more computationally efficient but less accurate for biomechanical simulation software, such as Anybody (www.anybodytech.com), OpenSim [2], and Artisynth [11], which integrate models and methods substantiated by experimental data.

Some massless muscle wire models include cylinders, spheres and ellipsoids, among others, to represent the bone surfaces of the skeleton around which the muscle is wrapped. However, general surface representations have been introduced through a parametric-based approach using the geodesic path on constrained motion manifolds [12], [13]. The most straightforward computation of the muscle-tendon path is the static via-point representation [14], which requires the definition of a set of constrained fixed points to pass through, connected by straight lines, [15]. This method yields low-fidelity muscle-tendon length and moment arms [16]. To overcome this limitation, [16] introduced a dynamic via-point representation by defining a joint-dependent set of points that considers the deflection of muscle-tendon path around bone surfaces.

For a more accurate representation of a muscle-tendon path, the skeletal structures in [17] are defined by geometrical shapes that model the constraint (bony contour) where the muscle-tendon wraps over. Although this method has been validated for cadaver samples, it isn't easy to obtain a subject-specific model due to the need for data from a more extensive set of specimens. The work in [9] follows a similar procedure, introducing the obstacle-set method and facilitating the scaling of the parameters for simpler geometries such as spheres and cylinders. However, the essential muscle-tendon velocity still needs to be addressed.

State-of-the-art muscle wrapping methods use geodesic theory to compute the shortest muscle-tendon path over tapered cylinders and ellipsoids [12]. Compared to the hybrid approximation technique used in Opensim, based on [18], the work in [12] provides a smoother solution, where the accuracy is compromised for specific joint configurations. Extension of [12] includes discrete multi-object wrapping paths [19]; however, depending on the resolution, the solutions may be less accurate than continuous solutions. Multi-object iterative formulations connect geodesics with straight-line segments, where geodesic unit normal vectors are used to compute straight lines tangent to the surface [13]. A disadvantage of this method is the need for a unique tangent direction (tangency) constraint, which leads to unfeasible solutions given the initial guess. Furthermore, its efficiency is diminished when using the effective Newton-Raphson method, with finite-differences Jacobians. Subsequent efficiency improvements that compute the analytical Jacobian using a single geodesic for a geometric obstacle were developed in [20] and [8]. The latter shows an explicit analytical computation of the muscle-tendon velocity. Unfortunately, due to the lack of tangency constraints, the analytical expression of muscle-tendon velocity needs to be corrected for some configurations, failing to comply with the minimum length muscle-tendon path. Some of these failing configurations may yield discontinuities at the connections between straight and curved-line segments, representing unrealistic paths. Additionally, discrete formulations allow to increase muscle-tendon length and velocity accuracy [6], [7], [21], but at the cost of increased computing time.

Consequently, novel methods are still needed to handle continuity along the entire path. Otherwise, incorrect computation of muscle-tendon path [21], and its velocity will lead to wrong muscle force production, regardless of using a state-of-the-art force model, such as Hill's. Such an anatomically consistent wrapping method will provide a reliable preliminary tool for biomechanical and human movement assessment and analysis.

III. Muscle Wrapping Modeling Over Parametric Surfaces

A. Problem Statement

Let the muscle wrapping be modeled considering the *i*-th muscle-tendon composed of $n+1$ straight-line segments (l_{S^i}) connected by n curved segments (l_{G^i}); thus, its total length can be obtained as

$$l^i_{MT} = \sum_{j=1}^{n+1} \left(l_{S^i_j} \right) + \sum_{j=1}^{n} \left(l_{G^i_j} \right). \tag{1}$$

Clearly, see Fig. 2, l^i_{MT} varies according to the position of the insertion ($\boldsymbol{a}^i_{n+1}$) and origin ($\boldsymbol{b}^i_0$) points and the pose (i.e., position and orientation) of the rigid bodies through which wrapping occurs. To continue, we need to assume the following:

1) the muscle's mass is negligible,
2) the muscle is taut at all time,

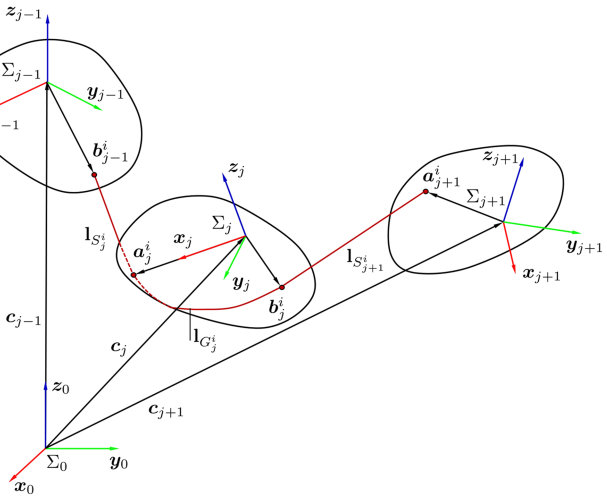

Fig. 2. Muscle wrapping over a rigid body: The muscle's origin and insertion points are represented by $\boldsymbol{b}^i_{j-1}$ and $\boldsymbol{a}^i_{j+1}$, respectively, where wrapping phenomenon occurs at the j-th surface.

3) the friction, between the muscle path and the wrapping surfaces, is negligible.

Thus, assuming the induced Euclidean norm $\| \boldsymbol{x} \|$ of any vector $\boldsymbol{x}$, the problem of *computing (1) involves the computation of* $n+1$ *straight-line lengths* $l_{S^i_j}$, n *geodesic lengths* $l_{G^i_j}$ *and* $2n$ *connection points* $\boldsymbol{a}^i_j, \boldsymbol{b}^i_j$ *that yields* $l^i_{MT} \in \mathcal{C}^1$*:*

B. Straight- and Curved-Line Segments Length

Consider the length of the straight-line segment given by $l_{S^i_j} = \| \boldsymbol{a}^i_j - \boldsymbol{b}^i_{j-1} \|$. The curved-line segment $l_{G^i_j}$ is represented by an arc length (s) parametrized curve, also known as unit speed curve, $\mathbf{r}(s) = \mathbf{r}(u(s), v(s)) : \mathbb{R}^2 \mapsto \mathbb{R}^3$, for $s_{a^i_j} \leq s \leq s_{b^i_j}$. Then, $\mathbf{r}(s)$ is a solution of the Euler-Lagrange equation [22]

$$\frac{d}{du}\frac{\partial f}{\partial v'} - \frac{\partial f}{\partial v} = 0 \tag{2}$$

with $f(u, v, v') = \sqrt{E + 2Fv' + Gv'^2}$, $v' = dv/du$ and $E = \mathbf{r}_u \cdot \mathbf{r}_u$, $F = \mathbf{r}_u \cdot \mathbf{r}_v$, $G = \mathbf{r}_v \cdot \mathbf{r}_v$, where subscript denotes partial derivatives. Equation (2) describes a unique geodesic determined by an initial point and its tangent. Hence, the curved segment is parametrized by surface coordinates (u, v), their derivatives with respect to arc length (u', v') that define the geodesic direction, and arc length s. For the *j*-th surface, and the *i*-th muscle, s takes the place of $l_{G^i_j}$ in (1).

C. Enforcing the Geodesic Unit Speed Constraint

A curve $\mathbf{r}(\alpha) = \mathbf{r}(u(\alpha), v(\alpha))$ is parametrized by the arc length if and only if

$$\| \bar{\mathbf{r}}(\alpha) \| = 1, \tag{3}$$

where bar $(\bar{\cdot})$ notation refers to the differentiation with respect to the parameter α. Condition (3) may not be fulfilled during the integration of the geodesic's differential equations, even if the initial conditions satisfy (3). In such a case, notice that when the curve $\mathbf{r}$ has not a unit speed, its tangent vector $\bar{\mathbf{r}}$ at some point p^i has two components of magnitudes $\bar{u}_{p^i}$ and $\bar{v}_{p^i}$, hence $\bar{\mathbf{r}}_{p^i}(\alpha) = \mathbf{r}_u \bar{u}_{p^i} + \mathbf{r}_v \bar{v}_{p^i}$, Therefore, to recover unicity, let the two magnitudes of unit tangent vector $\mathbf{t}_{p^i}$ be $\lambda_{p^i} = \frac{\bar{u}_{p^i}}{\|\bar{\mathbf{r}}_{p^i}\|}$ and $\mu_{p^i} = \frac{\bar{v}_{p^i}}{\|\bar{\mathbf{r}}_{p^i}\|}$, which are then normalized by $E\lambda^2_{p^i} + 2F\lambda_{p^i}\mu_{p^i} + G\mu^2_{p^i}$. Finally, the normalized λ_{p^i} and μ_{p^i} are treated subsequently as u'_{p^i} and v'_{p^i} [8], respectively, to yield a unit speed curve that complies to (3).

D. Derivation of the Muscle-Tendon Velocity

The calculation of the time derivative of a straight-line segment length yields

$$\dot{l}_{S^i_j} = \mathbf{l}_{S^i_j} \cdot \left({}^{(0)}\dot{\boldsymbol{a}}^i_j - {}^{(0)}\dot{\boldsymbol{b}}^i_{j-1} \right) \tag{4}$$

where left superscript ${}^{(m)}$ indicates an expression w.r.t Σ_m.

Consider the following integration for the time derivative of a curved wrapping segment length

$$l_{G^i_j} = \int_{\alpha_{a^i_j}}^{\alpha_{b^i_j}} \| \bar{\mathbf{r}}^i_j(\alpha) \| \, d\alpha \tag{5}$$

where $\mathbf{r}^i_j(\alpha_{a^i_j}) = {}^{(j)}\boldsymbol{a}^i_j$ and $\mathbf{r}^i_j(\alpha_{b^i_j}) = {}^{(j)}\boldsymbol{b}^i_j$. Taking the time derivative of (5) yields

$$\dot{l}_{G^i_j} = \frac{d}{dt}\int_{\alpha_{a^i_j}}^{\alpha_{b^i_j}} \| \bar{\mathbf{r}}^i_j(\alpha) \| \, d\alpha \tag{6}$$

$$= \frac{d\alpha}{dt}\left(\left\| \bar{\mathbf{r}}^i_j(\alpha_{b^i_j}) \right\| - \left\| \bar{\mathbf{r}}^i_j(\alpha_{a^i_j}) \right\| \right) \tag{7}$$

From the minimum l^i_{MT} length, i.e. $\nabla_\alpha l^i_{MT}(\alpha) = 0$, one obtains

$$\frac{\partial l^i_{MT}}{\partial \alpha_{a^i_j}} = \frac{\boldsymbol{a}^i_j - \boldsymbol{b}^i_{j-1}}{\| \boldsymbol{a}^i_j - \boldsymbol{b}^i_{j-1} \|} \cdot \bar{\mathbf{r}}^i_j(\alpha_{a^i_j}) - \left\| \bar{\mathbf{r}}^i_j(\alpha_{a^i_j}) \right\| = 0, \tag{8}$$

$$\frac{\partial l^i_{MT}}{\partial \alpha_{b^i_j}} = \frac{\boldsymbol{a}^i_{j+1} - \boldsymbol{b}^i_j}{\| \boldsymbol{a}^i_{j+1} - \boldsymbol{b}^i_j \|} \cdot \bar{\mathbf{r}}^i_j(\alpha_{b^i_j}) - \left\| \bar{\mathbf{r}}^i_j(\alpha_{b^i_j}) \right\| = 0. \tag{9}$$

Rewriting (8) and (9), results in the following expressions

$$\frac{\boldsymbol{a}^i_j - \boldsymbol{b}^i_{j-1}}{\| \boldsymbol{a}^i_j - \boldsymbol{b}^i_{j-1} \|} = \frac{\bar{\mathbf{r}}^i_j(\alpha_{a^i_j})}{\left\| \bar{\mathbf{r}}^i_j(\alpha_{a^i_j}) \right\|}, \tag{10}$$

$$\frac{\boldsymbol{a}^i_{j+1} - \boldsymbol{b}^i_j}{\| \boldsymbol{a}^i_{j+1} - \boldsymbol{b}^i_j \|} = \frac{\bar{\mathbf{r}}^i_j(\alpha_{b^i_j})}{\left\| \bar{\mathbf{r}}^i_j(\alpha_{b^i_j}) \right\|}. \tag{11}$$

Notice that (10) and (11) describe the tangency of the straight-line segments onto the surface, that is, it specifies the direction of vectors $\mathbf{l}_{S^i_j} = \mathbf{t}_{a^i_j}$ and $\mathbf{l}_{S^i_{j+1}} = \mathbf{t}_{b^i_j}$, where

$$\mathbf{l}_{S^i_j} = \frac{\boldsymbol{a}^i_j - \boldsymbol{b}^i_{j-1}}{\| \boldsymbol{a}^i_j - \boldsymbol{b}^i_{j-1} \|}. \tag{12}$$

Now, substituting the differentiation w.r.t time of ${}^{(j)}\boldsymbol{a}^i_j$ and ${}^{(j)}\boldsymbol{b}^i_j$ into the time derivatives of (8) and (9), respectively, the following expressions are obtained

$$\mathbf{l}_{S^i_j} \cdot {}^{(j)}\dot{\boldsymbol{a}}^i_j = \frac{d\alpha}{dt}\left\| \bar{\mathbf{r}}^i_j(\alpha_{a^i_j}) \right\| \tag{13}$$

$$\mathbf{l}_{S^i_{j+1}} \cdot {}^{(j)}\dot{\boldsymbol{b}}^i_j = \frac{d\alpha}{dt}\left\| \bar{\mathbf{r}}^i_j(\alpha_{b^i_j}) \right\| \tag{14}$$

Substituting (13) and (14) into (7) yields

$$\dot{l}_{G^i_j} = \left(\mathbf{l}_{S^i_{j+1}} \cdot {}^{(j)}\dot{\boldsymbol{b}}^i_j\right) - \left(\mathbf{l}_{S^i_j} \cdot {}^{(j)}\dot{\boldsymbol{a}}^i_j\right) \tag{15}$$

and considering ${}^{(0)}\dot{\boldsymbol{a}}^i_j = {}^{(0)}\dot{\boldsymbol{c}}_j + {}^{(j)}\dot{\boldsymbol{a}}^i_j$, and ${}^{(0)}\dot{\boldsymbol{b}}^i_j = {}^{(0)}\dot{\boldsymbol{c}}_j + {}^{(j)}\dot{\boldsymbol{b}}^i_j$, where ${}^{(0)}\boldsymbol{c}_j$ and ${}^{(0)}\dot{\boldsymbol{c}}_j$ are the position and velocity, respectively, of the origin of the j-th surface w.r.t Σ_0. Thus, the muscle-tendon velocity is obtained as follows

$$\begin{aligned} \dot{l}^i_{MT} = {} & \mathbf{l}_{S^i_{n+1}} \cdot {}^{(0)}\dot{\boldsymbol{a}}^i_{n+1} - \mathbf{l}_{S^i_1} \cdot {}^{(0)}\dot{\boldsymbol{b}}^i_0 \\ & + \sum_{j=1}^{n}\left(\mathbf{l}_{S^i_j} \cdot {}^{(0)}\dot{\boldsymbol{c}}_j - \mathbf{l}_{S^i_{j+1}} \cdot {}^{(0)}\dot{\boldsymbol{c}}_j\right) \end{aligned} \tag{16}$$

where $\dot{\boldsymbol{a}}^i_{n+1}$ and $\dot{\boldsymbol{b}}^i_0$ are the velocities of insertion and origin points, respectively. Equation (16) refers to the muscle-tendon velocity when the orientation of Σ_j is equal to the orientation of Σ_0. Considering the surface's rotational motion, the muscle-tendon velocity can be expressed as

$$\begin{aligned} \dot{l}^i_{MT} = {} & \mathbf{l}_{S^i_{n+1}} \cdot {}^{(0)}\dot{\boldsymbol{a}}^i_{n+1} - \mathbf{l}_{S^i_1} \cdot {}^{(0)}\dot{\boldsymbol{b}}^i_0 \\ & + \sum_{j=1}^{n}\Big(\mathbf{l}_{S^i_j} \cdot {}^{(0)}\dot{\boldsymbol{c}}_j + \mathbf{l}_{S^i_j} \cdot \hat{\boldsymbol{\omega}}_j \boldsymbol{R}_j {}^{(j)}\boldsymbol{a}^i_j \\ & - \mathbf{l}_{S^i_{j+1}} \cdot {}^{(0)}\dot{\boldsymbol{c}}_j - \mathbf{l}_{S^i_{j+1}} \cdot \hat{\boldsymbol{\omega}}_j \boldsymbol{R}_j {}^{(j)}\boldsymbol{b}^i_j\Big) \end{aligned} \tag{17}$$

where $\boldsymbol{R}_j$ and $\boldsymbol{\omega}_j$ are the rotation matrix from Σ_0 to Σ_j and the angular velocity of the j-th surface, respectively. The symbol $\hat{(\cdot)}$ denotes the skew-symmetric matrix operator over a 3 dimensional vector.

E. From/to Wrapping to/from Non-Wrapping Condition

A major issue in wrapping phenomenon is to handle transition to and from non-wrapping conditions. In the continuous domain, as in our case, it implies enforcing continuity at surface's contact points, where straight and geodesic segments meet. Then, we have the following result.

Proposition 1: Let insertion points $\boldsymbol{a}^i_{j+1}(t), \boldsymbol{b}^i_{j-1}(t), \in S_j$ connected by the continuous geodesic segment $l^i_{MT} \in \mathcal{C}^1$, for S_j the j-th smooth implicit surface $\varphi(\psi)_j = 0$ of j-th parametric smooth object. In virtue of tangency constraint is satisfied all over l^i_{MT}, including at its anchoring points $\boldsymbol{a}^i_{j+1}(t), \boldsymbol{b}^i_{j-1}(t)$, the infinitesimal continuous variation $\delta l^i_{MT} \to 0$ (where straight- and curved-line segments coincide) yields $\boldsymbol{a}^i_{j+1}(t) \to \boldsymbol{b}^i_{j-1}(t) \in \mathcal{C}^1$ continuously.

Proof: It follows straightforwardly from L'Hôpital's rule.

F. Tangency Constraint for a Unique Curved-Line Segment

In order to find the parameters u, v, u', v' and l_G for the j-th geodesic, let the tangency error function be modeled as a constraint-based on (10) and (11), to enforce $\mathcal{C}^1$ continuity at connection points $\boldsymbol{a}^i_j$ and $\boldsymbol{b}^i_j$:

$$\mathbf{f}(\mathbf{x}^{i,j}) = \begin{bmatrix} \mathbf{l}_{S^i_j} - \mathbf{t}_{a^i_j} \\ \mathbf{l}_{S^i_{j+1}} - \mathbf{t}_{b^i_j} \end{bmatrix} = 0 \tag{18}$$

where

$$\mathbf{x}^{i,j} = \begin{bmatrix} u_{a^i_j} & v_{a^i_j} & u'_{a^i_j} & v'_{a^i_j} & l_{G^i_j} \end{bmatrix}^T, \tag{19}$$

Now, in order to assess the numerical stability of the tangency-based constrained solution, three numerical methods are presented.

IV. Computation of Well-Posed Curved-Line Segments

The numerical solution of the curved-line segment length is assessed using the Newton-Raphson (NR) and two Quasi-Newton Methods (Broyden–Fletcher–Goldfarb–Shanno (BFGS) [23], and Broyden (BR) [24]); the later is considered to reduce the computational cost of $\mathbf{J}(\mathbf{x}^{i,j})$.

A. Newton-Raphson Formulation

The nonlinear tangency constraint (18) can be solved for $\mathbf{x}^{i,j}_k$ using the Newton-Raphson (NR) method by updating (19) as

$$\mathbf{x}^{i,j}_{k+1} = \mathbf{x}^{i,j}_k - \mathbf{J}^{-1}\left(\mathbf{x}^{i,j}_k\right)\mathbf{f}\left(\mathbf{x}^{i,j}_k\right). \tag{20}$$

The efficiency of the NR method relies mainly on the computation of the Jacobian $\mathbf{J}(\mathbf{x}^{i,j}) \in \mathbb{R}^{6\times 5}$, which depends on local and neighboring curves when they exist. Notice that evaluation of (18) needs both the computation of $\mathbf{l}_{S^i_j}$ and $\mathbf{t}_{a^i_j}$; moreover, given that $\mathbf{J}$ is a non-square matrix, the pseudo-inverse $\mathbf{J}^{\#} \in \mathbb{R}^{6\times 5}$ is used based on its regularization with a parameter $\lambda > 0$, given by

$$\mathbf{J}^{\#\lambda} = \left(\mathbf{J}^T\mathbf{J} + \lambda\mathbf{I}\right)^{-1}\mathbf{J}^T. \tag{21}$$

Then, (20) becomes in the following update rule

$$\mathbf{x}^{i,j}_{k+1} = \mathbf{x}^{i,j}_k - \mathbf{J}^{\#\lambda}\left(\mathbf{x}^{i,j}_k\right)\mathbf{f}\left(\mathbf{x}^{i,j}_k\right). \tag{22}$$

B. Broyden–fletcher–goldfarb–shanno Formulation

The objective is to minimize the tangency error squared norm

$$f(\mathbf{x}^{i,j}) = \left\|\mathbf{f}(\mathbf{x}^{i,j})\right\|_2^2, \tag{23}$$

by updating (19) as $\mathbf{x}^{i,j}_{k+1} = \mathbf{x}^{i,j}_k + \alpha_k\mathbf{d}_k$, for α_k the stepsize and $\mathbf{d}_k$ the descent direction. This latter vector $\mathbf{d}_k$ is determined by solving $\mathbf{B}_k\mathbf{d}_k + \nabla f\left(\mathbf{x}^{i,j}_k\right) = 0$, where matrix $\mathbf{B}_k$ stands for an approximation to the Hessian matrix at iteration k, and $\nabla f(\mathbf{x}^{i,j}_k)$ is the gradient at $\mathbf{x}^{i,j}_k$. The Hessian is computed by a rank-two update

$$\mathbf{B}_{k+1} = \mathbf{B}_k + \frac{\mathbf{y}_k\mathbf{y}_k^T}{\mathbf{y}_k^T\mathbf{s}_k} - \frac{\mathbf{B}_k\mathbf{s}_k\mathbf{s}_k^T\mathbf{B}_k^T}{\mathbf{s}_k^T\mathbf{B}_k\mathbf{s}_k} \tag{24}$$

for $\mathbf{s}_k = \mathbf{x}_{k+1} - \mathbf{x}_k$, and $\mathbf{y}_k = \nabla f(\mathbf{x}_{k+1}) - \nabla f(\mathbf{x}_k)$, and the inverse of the approximated Hessian matrix is obtained using

the Sherman–Morrison formula

$$\mathbf{B}_{k+1}^{-1} = \left(\mathbf{I} - \frac{\mathbf{s}_k \mathbf{y}_k^T}{\mathbf{y}_k^T \mathbf{s}_k}\right) \mathbf{B}_k^{-1} \left(\mathbf{I} - \frac{\mathbf{y}_k \mathbf{s}_k^T}{\mathbf{y}_k^T \mathbf{s}_k}\right) + \frac{\mathbf{s}_k \mathbf{s}_k^T}{\mathbf{y}_k^T \mathbf{s}_k}, \quad (25)$$

Notice that the evaluation of $\mathbf{B}_k^{-1}$ is avoided by initializing it with the identity matrix so that the first iteration is the gradient descent, then the subsequent iterations improve the estimation of $\mathbf{x}^{i,j}$. Stepsize α_k is determined using the next Procedure 1 to minimize f along the ray $\mathbf{x}_k^{i,j} + \alpha_k \mathbf{d}_k$, [25].

Procedure 1 (*Backtracking line search algorithm*)*:* Once the descent direction is obtained, α_k is determined by checking the Armijo condition

$$f\left(\mathbf{x}_k^{i,j} + \alpha_k \mathbf{d}_k\right) \leq f\left(\mathbf{x}_k^{i,j}\right) + a\alpha_k \mathbf{d}_k^T \nabla f\left(\mathbf{x}_k^{i,j}\right) \quad (26)$$

for a positive constant $a < 1$, and $\mathbf{d}_k^T \nabla f\left(\mathbf{x}_k\right)$ represents the directional derivative of f along $\mathbf{d}_k$, while stepsize $\alpha_k = b\alpha_{k-1}$, for positive constant $b < 1$, starting from a large stepsize α_0.

C. Broyden Formulation

The roots of (18) are found by updating vector $\mathbf{x}_k^{i,j}$ as

$$\mathbf{x}_{k+1}^{i,j} = \mathbf{x}_k^{i,j} + \beta_k \mathbf{p}_k \quad (27)$$

where β_k is the stepsize, and $\mathbf{p}_k$ is the quasi-Newton direction obtained by solving the linear system of equations $\mathbf{L}_k \mathbf{p}_k + \mathbf{f}\left(\mathbf{x}_k^{i,j}\right) = 0$, with $\mathbf{L}_k$ as an approximation to the Jacobian matrix evaluated at $\mathbf{x}_k^{i,j}$, and updated using

$$\mathbf{L}_{k+1} = \mathbf{L}_k + \theta_k \frac{\left(\mathbf{z}_k - \mathbf{L}_k \mathbf{u}_k\right) \mathbf{u}_k^T}{||\mathbf{u}_k||^2} \quad (28)$$

where $\mathbf{u}_k = \mathbf{x}_{k+1}^{i,j} - \mathbf{x}_k^{i,j}$, $\mathbf{z}_k = \mathbf{f}\left(\mathbf{x}_{k+1}^{i,j}\right) - \mathbf{f}\left(\mathbf{x}_k^{i,j}\right)$, and parameter θ_k is chosen such that $|\theta_k - 1| \leq \bar{\theta}$, with $\bar{\theta} \in (0, 1)$ and $\mathbf{L}_{k+1}$ is non singular. The stepsize β_k is determined by an Approximate Norm Descent Line Search [26], described in the next procedure.

Procedure 2 (*Derivative-free line search algorithm*)*:* Given $\eta, \sigma_1, \sigma_2 > 0$ and $\rho, \vartheta \in (0, 1)$, let $\beta_k = \vartheta^{i_k}$ for i_k the smallest non-negative integer such that

$$\begin{aligned} &||\mathbf{f}\left(\mathbf{x}_k^{i,j} + \beta_k \mathbf{p}_k\right)|| \leq ||\mathbf{f}\left(\mathbf{x}_k^{i,j}\right)|| \\ &-\sigma_1 ||\beta_k \mathbf{p}_k||^2 + \eta_k ||\mathbf{f}\left(\mathbf{x}_k^{i,j}\right)|| \end{aligned} \quad (29)$$

and η_k is a positive sequence satisfying $\sum_{k=0}^{\infty} \eta_k \leq \eta < \infty$. Notice that if $||\mathbf{f}\left(\mathbf{x}_k^{i,j} + \mathbf{p}_k\right)|| \leq \rho ||\mathbf{f}\left(\mathbf{x}_k^{i,j}\right)|| - \sigma_2 ||\mathbf{p}_k||^2$, then $\beta_k := 1$, otherwise, for $i = 0, 1, \ldots$, check the inequality (29) with $\beta_k = \vartheta^{i_k}$ successively.

V. Dynamic Simulations

Simulations were performed in MATLAB R2020b on an Intel Core i5-10500H @2.50 GHz with 16 GB RAM running 64-bit Windows 10 Pro. The MATLAB code used in this letter, and simulation videos, can be downloaded at https://github.com/irammunoz/Muscle-tendon-Wrapping. The simulations' duration was 3 s with a constant time step $h = 0.012$ s.

A. Modeling Muscle Wrapping Over One Cylinder

The proposed method is first tested considering the wrapping of a muscle-tendon unit around a cylinder surface, with $\boldsymbol{b}_0^1$ and $\boldsymbol{a}_2^1$ as the origin and insertion muscle points, respectively. The cylinder of radius r is parametrized in the local coordinate frame Σ_1 using u and v coordinates as $\mathbf{r}(u, v) = \begin{bmatrix} r\cos u & r\sin u & v \end{bmatrix}^T$ whose coordinates $(x(u, v), y(u, v), z(u, v))$ are translated w.r.t its parent coordinate frame Σ_0. Two cases were simulated considering fixed origin and insertion points for one muscle-tendon path:

Case 1: The muscle-tendon unit remains in contact with the cylindrical surface, while the cylinder follows a sinusoidal trajectory: ${}^{(0)}\mathbf{c}(t) = \begin{bmatrix} 0 & 0.009\sin(2\pi t) & 0 \end{bmatrix}$.

Case 2: The muscle-tendon unit transitions from a wrapping state to a non-wrapping state (using the cylinder non-wrapping condition presented in [9]), while the cylinder follows a sinusoidal trajectory: ${}^{(0)}\mathbf{c}(t) = \begin{bmatrix} 0 & 0.02\sin(2\pi t) & 0 \end{bmatrix}$.

Case 1 and 2 were simulated using the NR, BFGS and BR methods, to analyze their numerical efficiency. In all simulations, the states were initialized to an unfeasible initial guess such that $||\mathbf{f}(\mathbf{x}_0)|| = 1.7086$. The following parameters were used for each numerical method:

- NR formulation: It finds the roots of (18) by updating (19) with (22) and (21), for $\lambda = 0.08, 0.1, 0.5$.
- BFGS formulation: It minimizes (23) and it was initialized with $\mathbf{B}_0^{-1} = \mathbf{I}$ and tested with and without Procedure 1, using $a = 0.382$ and $b = 0.618$.
- BR formulation: It finds the roots of (18) updating (19) with (27). $\mathbf{L}_0$ was initialized using central finite differences to approximate $\mathbf{J}$; θ_k was set to 1. It was tested with and without Procedure 2 setting $\sigma_1 = 0.001$, $\sigma_2 = 0.001$, $\rho = 0.9$, $\vartheta = 0.5$ and $\eta_k = 1/(k+1)^2$.

The Jacobian $\mathbf{J}$ and the gradient needed by the NR and BFGS methods, respectively, were approximated using finite differences. Numerical methods were terminated when $||\mathbf{f}(\mathbf{x}^{i,j})|| \leq$ 1.0E-10 occurred.

B. Modeling Muscle Wrapping Over Two Cylinders

The simulation aims at testing the proposed wrapping method with two cylinders using the BR method, and the same parameters for this method as in the simulation over one cylinder. The multi-obstacle wrapping case was simulated considering fixed origin and insertion points for one muscle-tendon path. The simulation considered the muscle-tendon unit transitions from/to a wrapping state to/from a non-wrapping state (using the cylinder non-wrapping condition presented in [9]), while the cylinders follow sinusoidal trajectories: ${}^{(0)}\mathbf{c}_1(t) = \begin{bmatrix} 0 & 0.15\sin(2\pi t) & 0 \end{bmatrix}$, ${}^{(0)}\mathbf{c}_2(t) = \begin{bmatrix} -0.5 & 0.15\cos(2\pi(t + 0.24)) & 0 \end{bmatrix}$.

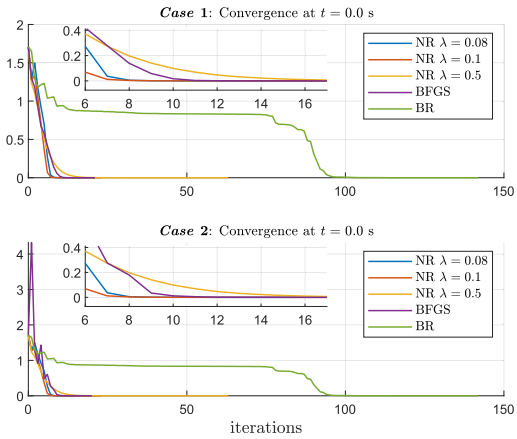

Fig. 3. Convergence rate of NR, BFGS, and BR methods at initialization.

For n surfaces, the total i-th muscle path tangency error can be described by

$$\boldsymbol{\phi}(\boldsymbol{\psi}) = \begin{bmatrix} \mathbf{f}(\mathbf{x}^{i,0}, \mathbf{x}^{i,1}, \mathbf{x}^{i,2}) \\ \mathbf{f}(\mathbf{x}^{i,1}, \mathbf{x}^{i,2}, \mathbf{x}^{i,3}) \\ \vdots \\ \mathbf{f}(\mathbf{x}^{i,n-1}, \mathbf{x}^{i,n}, \mathbf{x}^{i,n+1}) \end{bmatrix} = \mathbf{0}, \tag{30}$$

where the roots of (30) can be find by updating the vector $\boldsymbol{\psi} = [\,\mathbf{x}^{i,0} \quad \mathbf{x}^{i,1} \quad \cdots \quad \mathbf{x}^{i,n}\,]$. Note that $\mathbf{x}^{i,0}$ and $\mathbf{x}^{i,n+1}$ can be dropped if the origin and insertion points do not depend on the parameters of geodesics. BR method was terminated when $\left|\left|\boldsymbol{\phi}(\boldsymbol{\psi})\right|\right| \leq$ 1.0E-10 occurred.

VI. Results

A. Muscle Wrapping Over One Cylinder

Fig. 3 shows the initial convergence of each method at $t = 0.0$ s for *Case* 1 and 2. The BFGS method shows slower convergence (11 iterations) than the NR method (7 iterations, $\lambda = 0.1$), whereas the BR method is slower (100 iterations). This convergence stands indeed for offline computation of Jacobian, used afterward as the initialized state. In this sense, although BR was slower to converge to a well-posed initial state $\mathbf{x}_0$, it shows the best numerical efficiency afterward. Numerical efficiency is assessed in terms of the number of total iterations (n_i), the average number of iterations per time step (i_a), and the number of function evaluations (n_f), for a given error tolerance. Table I shows the overall efficiency results, wherein the BR method outperforms BFGS and NR methods. The BR method (using the derivative-free line search algorithm) requires the fewest number of function evaluations (n_f) for both *Cases* (10,100 and 10,264, respectively); with the fewer average of iterations per time step (i_a) using 13 and 14 iterations, respectively. However, less computation time (t_a), measured with the *timeit* MATLAB's function, is obtained using a $\beta = 1.0$. As the results show that BR is the best method, from now on only simulations results with this method are shown. The muscle-tendon path solution obtained with the BR method for Case 1 and 2 are shown in Figs. 4 and 5,

TABLE I
Results for Each Muscle-Tendon Case and Solving Method

Case	Method	Parameter	n_i	i_a	n_f	t_a
1	NR	$\lambda = 0.08$	4,273	17	47,254	18.07
		$\lambda = 0.1$	4,870	19	53,821	21.51
		$\lambda = 0.5$	14,382	57	158,453	69.36
	BFGS	$\alpha = 1.0$	4,091	16	88,672	50.43
		$\alpha \leftarrow$ Proc. 1	3,516	14	78,423	48.61
	BR	$\beta = 1.0$	16,772	66	19,533	3.53
		$\beta \leftarrow$ Proc. 2	3,464	13	10,100	5.30
2	NR	$\lambda = 0.08$	4,429	17	48,970	17.56
		$\lambda = 0.1$	4,997	19	55,218	20.38
		$\lambda = 0.5$	15,912	63	175,283	64.13
	BFGS	$\alpha = 1.0$	4,386	17	94,867	54.96
		$\alpha \leftarrow$ Proc. 1	3,872	15	85,976	54.23
	BR	$\beta = 1.0$	16,854	67	19,615	3.58
		$\beta \leftarrow$ Proc. 2	3,546	14	10,264	5.51

n_i: Total number of iterations
i_a: Average number of iterations per time step (rounded-off value)
n_f: Total number of function evaluations
t_a: Average computation time in seconds

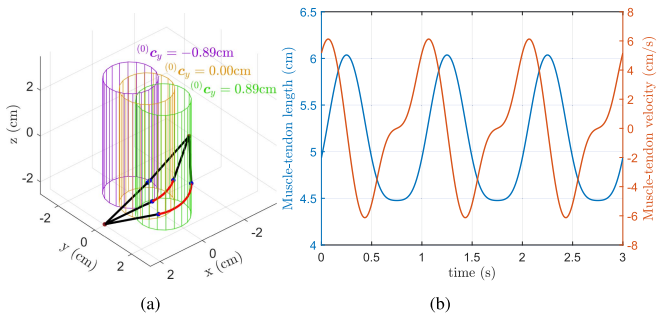

Fig. 4. Cylinder moves only along $y-$axis ($c_y = 0.009\sin(2\pi t)$): Path obtained with the Broyden method for *Case* 1 with an initial guess $\left|\left|\mathbf{f}(\mathbf{x}_0)\right|\right| = 1.7086$; (a) render of muscle wrapping path at $t = 0$ s (yellow), $t = 0.24$ s (green), and $t = 0.744$ s (purple); (b) muscle-tendon length and its velocity over time.

respectively. There can be seen that the muscle-tendon length in both cases follows a sinusoidal path during the wrapping state, and remains constant at some intervals in *Case* 2 when the muscle-tendon is not in compliant motion with the cylinder. Moreover, results are accurate in comparison to the obstacle-set method [9], with a maximum error below 15.0E-11 cm for both *Case* 1 and *Case* 2, as shown in Fig. 6. Note that in both cases, $\mathcal{C}^1$ continuity is guaranteed using arbitrary initial conditions. An animation of each simulation case can be found in the online supplementary material, where also an additional animation shows the translational and rotational motion of the surface.

B. Muscle Wrapping Over Two Cylinders

For the case of wrapping over two cylinders, the BR method was used with $\beta = 1.0$, as the best results were obtained in the case of one cylinder (see Table I). Results showed that for an initial guess $\boldsymbol{\psi}_0$ such that $\left|\left|\boldsymbol{\phi}(\boldsymbol{\psi}_0)\right|\right| = 1.3043$, the BR method required a total of 3297 iterations (n_i), 6058 function evaluations (n_f), with an average of 13 iterations per time step (i_a) and a total

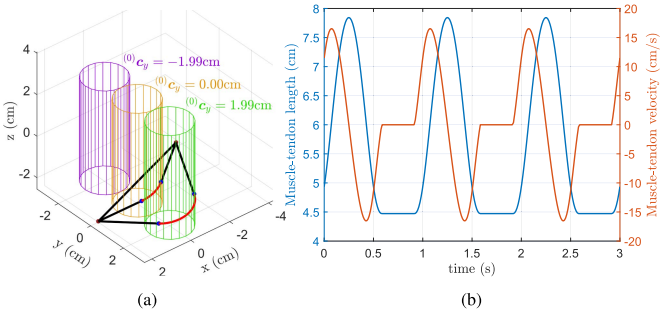

Fig. 5. Cylinder moves only along $y-$axis ($c_y = 0.02\sin(2\pi t)$): Path obtained with the Broyden method for *Case* 2 with an initial guess $\left|\left|\mathbf{f}(\mathbf{x}_0)\right|\right| = 1.7086$; (a) render of muscle wrapping path at $t = 0$ s (yellow), $t = 0.24$ s (green), and $t = 0.744$ s (purple); (b) smooth muscle-tendon length and its velocity over time.

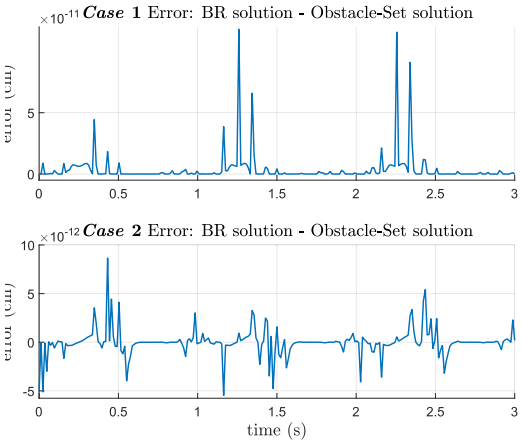

Fig. 6. Error of muscle-tendon length between the BR and the obstacle-set methods [9].

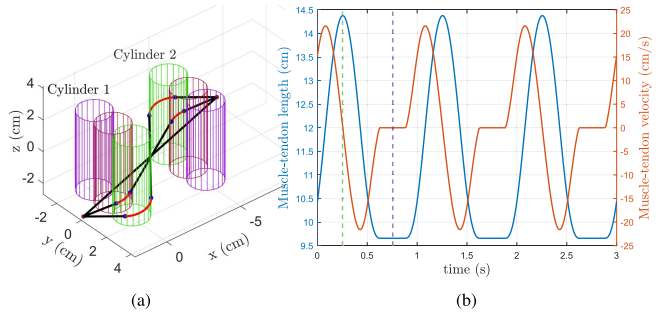

Fig. 7. Cylinders move only along $y-$axis ($c_{1y} = 0.15\sin(2\pi t)$, $c_{2y} = 0.15\sin(2\pi(t + 0.24))$): Path obtained with the Broyden method with an initial guess $\left|\left|\boldsymbol{\phi}(\boldsymbol{\psi}_0)\right|\right| = 1.3043$; (a) render of muscle wrapping path at $t = 0$ s (dark red), $t = 0.252$ s (green), and $t = 0.756$ s (purple); (b) smooth muscle-tendon length and its velocity over time.

computation time (t_a) of 9.1707 s. During the whole simulation, muscle-tendon path $\mathcal{C}^1$ continuity was guaranteed, see Fig. 7.

VII. Discussions

Our proposed method shows the $\mathcal{C}^1$ continuity required to compute a well-posed muscle-tendon velocity; therefore, our proposal is suitable for the computation of the musculoskeletal

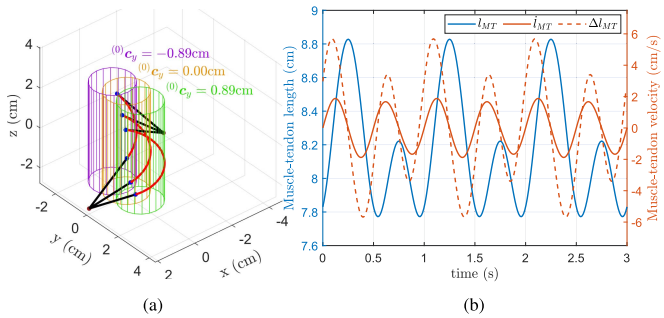

Fig. 8. Newton-Raphson method solution for *Case* 1 yields ill-posed configurations using [8], for an initial guess $\mathbf{x}_0$ such that $\left|\left|\mathbf{f}(\mathbf{x}_0)\right|\right| = 0.9401$; (a) muscle wrapping path at $t = 0$ s (yellow), $t = 0.24$ s (green), and $t = 0.744$ s (purple) and (b) muscle-tendon length and velocity over time.

production of contraction force, which is essential for biomechanical models at the dynamic level. Let us analyze this claim further. The state-of-the-art method [8] guarantees $\mathcal{C}^0$ by enforcing the geodesic's normal $\mathbf{N}$ and binormal $\mathbf{B}$ vectors, at points $\boldsymbol{a}_j^i$ and $\boldsymbol{b}_j^i$, be orthogonal to a straight-line segment based on the following dot product constraint, without involving tangent vectors,

$$\mathbf{f}(\mathbf{x}^{i,j}) = \begin{bmatrix} \mathbf{l}_{S_j^i} \cdot \mathbf{B}_{a_j^i} \\ \mathbf{l}_{S_j^i} \cdot \mathbf{N}_{a_j^i} \\ \mathbf{l}_{S_{j+1}^i} \cdot \mathbf{B}_{b_j^i} \\ \mathbf{l}_{S_{j+1}^i} \cdot \mathbf{N}_{b_j^i} \end{bmatrix} = \mathbf{0}. \tag{31}$$

This formulation may include non-physiological muscle-tendon configurations, such as muscle "folding". To illustrate this, we have simulated *Case* 1 based on (31) using the NR method, see Fig. 8(a). Therein, a non-shortest muscle path is obtained, representing an unrealistic (non-physiological) muscle-tendon configuration, which is avoided using our proposed tangency constraints (18) or (23). Furthermore, the computation of the muscle-tendon velocity (16), which is equal to the one presented in [8], is not consistent with the whole set of solutions provided by (31), but only when the tangency constraints are satisfied. This inconsistency is shown in Fig. 8(b) that depict velocities obtained with (16) ($\dot{l}_{MT}^i$, orange solid line) versus finite differences (Δl_{MT}, orange dashed line). It is worth mentioning that the analytical expression for the Jacobian of [8], derived using (31), requires indeed a $\mathcal{C}^1$ formulation, which can be obtained with an initial guess in the vicinity of a solution that satisfies tangency constraints. Even though $\mathcal{C}^1$ continuity is guaranteed with our method, choosing an appropriate initial guess is required; otherwise, different wrapping directions may arise, as described in [9]. Then, for large-scale formulations (considering multiple obstacles or muscles) an automatic method to initialize the algorithm needs to be developed.

Intending to simplify the clarity of the figures, the first simulations and results presented were for only one muscle and one cylinder, though our formulation and algorithms have been developed to be extended to a set of n contact surfaces. Indeed, the second part of simulations were about the wrapping over two cylinders, demonstrating that readiness of the proposed framework.

VIII. Conclusion and Future Work

A method based on tangency constraints of geodesic paths has been proposed that guarantees continuous muscle wrapping around parametric surfaces. This latter is essential to calculate the shortest muscle-tendon path during a wrapping condition and thus achieve accurate biomechanical modeling of muscle forces. Simulations showed $\mathcal{C}^1$ geodesic muscle-tendon paths in two cases: 1) remaining in a wrapping state and 2) transitioning to a wrapping from a non-wrapping state. Furthermore, unlike other works, the numerical efficiency of the commonly used NR method and two quasi-Newton methods were studied. Results show the proposed method's effectiveness in guaranteeing the continuous computation of the muscle-tendon path and a fast-solving procedure using the quasi-Newton Broyden's method. In this realm, the contribution of this work ranges from calculating the shortest muscle-tendon path in a wrapping condition to the analytical solution of the muscle-tendon velocity; both quantities are necessary when using the well-known classical Hill-type actuation muscle model, which is fundamental in advanced biomechanical studies. In contrast to the literature, the $\mathcal{C}^1$ continuous solution of our method is obtained using as a constraint the unit tangent vectors of the geodesic.

Immediate future work is in three venues, to speed up the algorithm, which can be improved by deriving an analytical expression for the NR Jacobian; to validate in a dynamic framework for a complex human musculoskeletal system based on the Hill actuation model, and to study how to handle the numerical commutation condition (to/from wrapping) at a lower sampling rate. A first validation of our formulation on a simple yet representative musculoskeletal model was presented in [27], where a comparison versus OpenSim, which uses an approximation of muscle-tendon velocity, showed differences in muscle-related quantities, joint motion, and joint torques. Therefore, our proposal contributes as a baseline to musculoskeletal modeling for human movement assessment. Also, as a byproduct of our proposed method, it can be extended to other wrapping applications, such as cable-driven robots, either rigid or soft ones, where an accurate description of cable path length is required.

References

[1] M. S. Shourijeh, N. Mehrabi, J. J. McPhee, and B. J. Fregly, "Editorial: Advances in musculoskeletal modeling and their application to neurorehabilitation," *Front. Neurorobot.*, vol. 14, 2020, Art. no. 65.

[2] A. Seth et al., "OpenSim: Simulating musculoskeletal dynamics and neuromuscular control to study human and animal movement," *PLoS Comput. Biol.*, vol. 14, no. 7, 2018, Art. no. e1006223.

[3] F. E. Zajac, "Muscle and tendon: Properties, models, scaling, and application to biomechanics and motor control," *Crit. Rev. Biomed. Eng.*, vol. 17, no. 4, pp. 359–411, 1989.

[4] C. Quental, J. Folgado, J. Ambrósio, and J. Monteiro, "A multibody biomechanical model of the upper limb including the shoulder girdle," *Multibody Syst. Dyn.*, vol. 28, no. 1, pp. 83–108, 2012.

[5] E. M. Arnold, S. R. Ward, R. L. Lieber, and S. L. Delp, "A model of the lower limb for analysis of human movement," *Ann. Biomed. Eng.*, vol. 38, no. 2, pp. 269–279, 2010.

[6] O. Zarifi and I. Stavness, "Muscle wrapping on arbitrary meshes with the heat method," *Comput. Methods Biomech. Biomed. Eng.*, vol. 20, no. 2, pp. 119–129, 2017.

[7] J. E. Lloyd, F. Roewer-Després, and I. Stavness, "Muscle path wrapping on arbitrary surfaces," *IEEE Trans. Biomed. Eng.*, vol. 68, no. 2, pp. 628–638, Feb. 2021.

[8] A. Scholz et al., "A fast multi-obstacle muscle wrapping method using natural geodesic variations," *Multibody Syst. Dyn.*, vol. 36, no. 2, pp. 195–219, 2016.

[9] B. A. Garner and M. G. Pandy, "The obstacle-set method for representing muscle paths in musculoskeletal models," *Comput. Methods Biomech. Biomed. Eng.*, vol. 3, no. 1, pp. 1–30, 2000.

[10] J. D. Webb, S. S. Blemker, and S. L. Delp, "3D finite element models of shoulder muscles for computing lines of actions and moment arms," *Comput. Methods Biomech. Biomed. Eng.*, vol. 17, no. 8, pp. 829–837, 2014.

[11] J. E. Lloyd, I. Stavness, and S. Fels, *ArtiSynth: A Fast Interactive Biomechanical Modeling Toolkit Combining Multibody and Finite Element Simulation*. Berlin, Heidelberg, Germany: Springer, 2012.

[12] S. P. Marsden and D. C. Swailes, "A novel approach to the prediction of musculotendon paths," *Proc. Inst. Mech. Eng., Part H: J. Eng. Med.*, vol. 222, no. 1, pp. 51–61, 2008.

[13] I. Stavness, M. Sherman, and S. Delp, "A general approach to muscle wrapping over multiple surfaces," in *Proc. Amer. Soc. Biomech.*, Gainsville, FL, USA, Aug. 15–18, 2012.

[14] S. Delp, J. P. Loan, M. G. Hoy, F. E. Zajac, E. L. Topp, and J. M. Rosen, "An interactive graphics-based model of the lower extremity to study orthopaedic surgical procedures," *IEEE Trans. Biomed. Eng.*, vol. 37, no. 8, pp. 757–767, Aug. 1990.

[15] J. Guo et al., "Modeling muscle wrapping and mass flow using a mass-variable multibody formulation," *Multibody Syst. Dyn.*, vol. 49, no. 3, pp. 315–336, 2020.

[16] A. B. Carman and P. D. Milburn, "Dynamic coordinate data for describing muscle–tendon paths: A mathematical approach," *J. Biomech.*, vol. 38, no. 4, pp. 943–951, 2005.

[17] F. C. T. Van der Helm et al., "Geometry parameters for musculoskeletal modelling of the shoulder system," *J. Biomech.*, vol. 25, no. 2, pp. 129–144, 1992.

[18] F. C. T. van der Helm, "The shoulder mechanism: A dynamical approach," Ph.D. dissertation, Delft Univ. Technol., Delft, The Netherlands, 1991.

[19] S. P. Marsden, D. C. Swailes, and G. R. Johnson, "Algorithms for exact multi-object muscle wrapping and application to the deltoid muscle wrapping around the humerus," *Proc. Inst. Mech. Engineers, Part H: J. Eng. Med.*, vol. 222, no. 7, pp. 1081–1095, 2008.

[20] A. Scholz et al., "Improved muscle wrapping algorithms using explicit path-error Jacobians," in *Computational Kinematics*. The Netherlands: Springer, 2014, pp. 395–403.

[21] J. Penner and S. Leyendecker, "A discrete mechanics approach for musculoskeletal simulations with muscle wrapping," *Multibody Syst. Dyn.*, vol. 56, no. 3, pp. 267–287, 2022.

[22] D. J. Struik, *Lectures on Classical Differential Geometry*. New York, NY, USA: Dover, 1988.

[23] R. Fletcher, *Practical Methods of Optimization*, 2nd ed. Hoboken, NJ, USA: Wiley, 2000.

[24] C. G. Broyden, "A class of methods for solving nonlinear simultaneous equations," *Math. Comput.*, vol. 19, pp. 577–593, 1965.

[25] J. Nocedal and S. J. Wright, *Numerical Optimization*, (Series in Operations Research and Financial Engineering Series), 2nd ed. New York, NY, USA: Springer, 2006.

[26] D.-H. Li and M. Fukushima, "A derivative-free line search and global convergence of Broyden-like method for nonlinear equations," *Optim. Methods Softw.*, vol. 13, no. 3, pp. 181–201, 2000.

[27] I. M. Pepi, N. Garcia-Hernandez, and V. Parra-Vega, "Forward neuromusculoskeletal dynamics with continuous muscle wrapping," *IEEE Robot. Automat. Lett.*, vol. 8, no. 9, pp. 5942–5949, Sep. 2023.

Open Access funding provided by 'Istituto Italiano di Tecnologia' within the CRUI CARE Agreement.